Field dependence of antiferromagnetic domain switching in epitaxial Fe/CoO/MgO(001) systems

Q. Li,[1,2] T. P. Ma,[1] M. Yang,[2] L. Sun,[1] S. Y. Huang,[1] R. W. Li,[3] C. Won,[4] Z. Q. Qiu,[2] and Y. Z. Wu[1,5,*]

[1]*Department of Physics and State Key Laboratory of Surface Physics, Fudan University, Shanghai 200433, People's Republic of China*
[2]*Department of Physics, University of California at Berkeley, Berkeley, California 94720, USA*
[3]*Chinese Academy of Sciences, Ningbo Institute of Materials Technology and Engineering, Key Laboratory of Magnetic Materials and Devices, Ningbo 315201, Zhejiang, People's Republic of China*
[4]*Department of Physics, Kyung Hee University, Seoul 130-701, Republic of Korea*
[5]*Collaborative Innovation Center of Advanced Microstructures, Nanjing 210093, China*

Utilizing the magneto-optic Kerr effect and Kerr microscopy measurements, we investigated the antiferromagnetic (AFM) domain switching process at different magnetic fields in a single-crystalline Fe/CoO bilayer grown on MgO(001) substrate. In spite of the zero-net magnetic moment in the CoO layer, we find that the activation energy barrier of CoO AFM domain switching decreased at larger magnetic field. To separate the different behaviors of domain nucleation and domain wall motion during the CoO spin switching process, a new analytical method was developed. Using this method, we found that the CoO domain nucleation energy barrier exhibited a jump at a critical magnetic field while the CoO domain wall motion experienced only a tiny energy barrier variation. The field-dependent behaviors of the energy barriers were attributed to the formation of a spiral domain wall in the Fe layer during its magnetization reversal and this was supported by micromagnetic simulations.

I. INTRODUCTION

The dynamics of magnetization reversal in magnetic thin films is of great interest due to its application in spintronic devices and for a fundamental understanding of magnetism [1–4]. For ferromagnetic (FM) materials, the energy barrier associated with magnetization reversal is known to be related to the magnetic field [1–3,5–7], temperature [1–5], electrical current [7,8], dimensions [9], the atomic morphology of the substrate [10], etc. In contrast, antiferromagnetic (AFM) magnetization reversal has been much less explored, despite its wide application in magnetic data storage and sensor devices [11]. There is evidence that many important properties, such as electrical transport in AFM materials, can be largely influenced by AFM spin configurations [12,13]. Very recently, AFM materials have also been employed in the generation, transport, and detection of spin current [14–18] for future spintronic devices. Since AFM spin configuration and domain switching are widely involved in spintronics technology, it is of great interest to study the AFM domain switching process especially in FM/AFM systems, where the FM magnetization switching is highly correlated with AFM magnetization switching.

AFM domain evolution has been previously explored to a certain extent in the exchange bias phenomenon as a function of time (usually referred to as the training effect) [19–22]. However, the random spin orientations of AFM polycrystalline grains, which are usually employed for such studies, complicate the spin switching, prohibiting an explicit exploration of the AFM spin switching process. Using single-crystalline Fe/CoO bilayers, it was recently demonstrated that the CoO AFM domain switching process can be revealed by the evolution of the Fe remanent state [23]. It was found that the AFM CoO spin switching in the Fe/CoO

system is characterized by an energy barrier dominated by thermal excitations. However, how to control AFM spin switching remains a big issue. Despite the observation of these temperature-dependent thermal excitations, there have been very few reports on how to control AFM spin switching (e.g., using a current-induced field to switch the AFM spins [24]). In this paper, we report magnetic field control of the energy barrier for CoO AFM spin switching in a coupled Fe/CoO bilayer. In spite of the zero-magnetic moment in the CoO AFM layer, the excitation energy barrier for CoO AFM domain switching was demonstrated to decrease in a larger field. Different contributions from domain nucleation and domain wall motion in the CoO AFM domain switching process can be separated as a function of magnetic field based on our new analytical method. We attributed this field-dependent behavior of the energy barrier to the formation of an exchange spring in the Fe layer, which is supported by micromagnetic simulation.

II. EXPERIMENTS

Fe/CoO/MgO(001) films were prepared in an ultrahigh vacuum (UHV) system by molecular beam epitaxy. The MgO(001) single-crystal substrates were cleaned with acetone, followed by annealing at 600 °C for half an hour inside a UHV chamber. A 10-nm MgO seed layer was deposited at 500 °C before the Fe/CoO growth. The 5-nm CoO film was grown by reactive deposition of Co at an oxygen pressure of 1.0×10^{-6} Torr at room temperature [25,26]. Subsequently, a 25-nm Fe film was grown on top of the CoO layer. Sharp reflection high-energy electron diffraction patterns revealed excellent epitaxy growth of Fe and CoO films with the lattice relation of Fe[100]‖CoO[110]‖MgO[110] [23,25,26]. Finally, this sample was capped with 4 nm MgO as a protective layer. The magnetic hysteresis loops of Fe films were measured by longitudinal magneto-optic Kerr effect (MOKE), in which the magnetic field was applied in the optical plane [Fig. 1(a)]. A
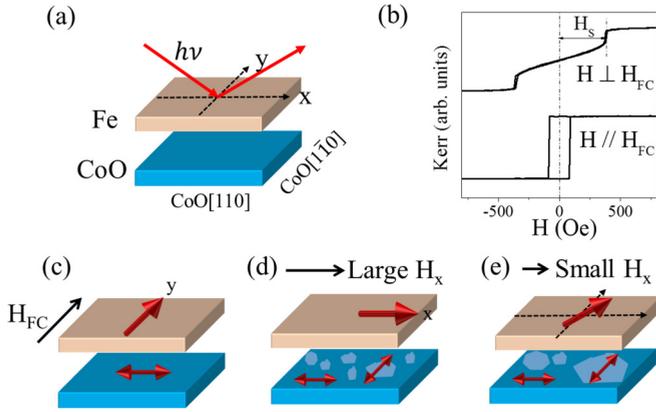
*wuyizheng@fudan.edu.cn

FIG. 1. (a) Schematic of longitudinal MOKE measurement geometry. (b) Hysteresis loops for $H \perp H_{FC}$ and $H \parallel H_{FC}$ from Fe (25 nm)/CoO (5 nm)/MgO(001) at 82 K. (c) Schematic of spin configuration in a Fe/CoO bilayer after field cooling and CoO AFM domain switching with (d) large range of field sweeping and (e) small range of field sweeping perpendicular to the field cooling direction. All the Fe and CoO spins are in the film plane.

vector magnet was used here, allowing in-plane field cooling both perpendicular and parallel to the field scanning direction. The maximum field of our vector magnet is 1400 Oe. The wavelength of the laser diode for MOKE measurement is 670 nm with the beam diameter $\sim$0.2 mm. Sample temperatures could be varied between 82 and 330 K in a small optical Dewar cooled by liquid nitrogen. Magnetic domain images were taken with commercial Kerr microscopy from the Evicomagnetics company. In this instrument, longitudinal MOKE was measured with an in-plane rotatable magnet.

III. RESULTS AND DISCUSSION

It is well known that CoO contains the G-type AFM spin structure, and the CoO(001) surface is spin compensated, thus Fe FM spins and CoO AFM spins are perpendicularly coupled in an Fe/CoO(001) system, commonly referred to as the spin-flop coupling [23,27]. Thus if a sample is cooled down with the cooling field H_{FC} along the Fe$\langle 100 \rangle$ direction, the CoO AFM spins should be aligned perpendicular to H_{FC} [Fig. 1(c)], and the spin-flop coupling between the Fe and CoO spins induce an in-plane uniaxial anisotropy in Fe film with the easy axis along H_{FC}, as proven by the hysteresis loop measurement shown in Fig. 1(b) [28,29]. The magnitude of this uniaxial anisotropy can be retrieved from the splitting field $H_S \approx 350$ Oe, defined as the offset field of the minor loop in the HA double-split loop in Fig. 1(b). Due to the compensated spin configuration on the CoO(001) surface, the exchange bias in Fe/CoO/MgO(001) is negligible if compared with the much stronger uniaxial anisotropy. However, as demonstrated in Ref. [23], CoO AFM spins can be switched by 90° by continuously sweeping the field perpendicular to H_{FC} due to strong interface exchange coupling and thermal activation [Figs. 1(c) and 1(d)]. Combining hysteresis loop, Kerr microscope, and x-ray magnetic linear dichroism measurements, the CoO AFM switching was investigated both directly and indirectly through the Fe layer, in which the remanence Kerr signal can be used to
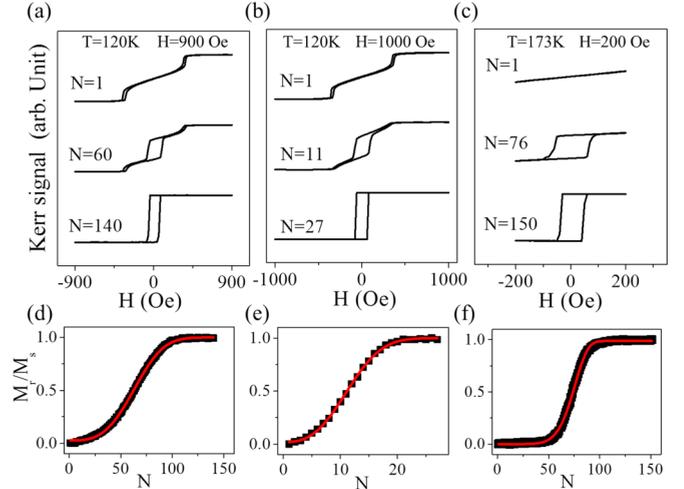

FIG. 2. Representative hysteresis loops for $H \perp H_{FC}$ during magnetic field cycling using a field sweeping range of (a) 900 Oe at 120 K, (b) 1000 Oe at 120 K, and (c) 200 Oe at 173 K. N denotes the cycling number. Before taking cycles of field scanning at each temperature, the sample was warmed to 330 K and field cooled to 80 K with $H_{FC} = 1000$ Oe. (d)–(f) The remanent Kerr signal in panels (a)–(c) increases with the cycling number. The red lines in panels (d)–(f) are the fitting result using Eq. (1).

represent the fractional area of the switched CoO spins due to the strongly coupled domains [23]. In this paper, we reported the study of how the CoO AFM domain switching depends on the strength of the sweeping field. We found the AFM domain switching occurred even for magnetic fields smaller than H_S [Fig. 1(e)] and the magnetic-field-dependent AFM domain switching process.

Figure 2 shows the typical hysteresis loops with different maximum field strength for $H \perp H_{FC}$ at selected temperatures. It is clear that cycling of the magnetic field gradually switched the in-plane easy axis of the Fe film by 90° from EA $\parallel H_{FC}$ to EA$\perp H_{FC}$, which originates from the underlying CoO AFM domain switching under thermal excitation [23]. The required loop cycling number to fully switch the CoO AFM domains for $H = 900$ Oe [Fig. 2(a)] is about three times larger than that with the sweeping field of 1000 Oe [Fig. 2(b)]. This result clearly demonstrates that CoO AFM domain switching strongly depends on the applied magnetic field strength, and a stronger field can switch the CoO AFM domain more easily.

CoO AFM domain switching can be understood by considering interface exchange coupling. As indicated in Fig. 1(d), when the strong field aligns the Fe moment along H ($H \perp H_{FC}$), spin-flop coupling drives the CoO AFM spin from the initial direction parallel to H to the direction perpendicular to H. However, we found that CoO AFM domain switching does not necessarily require alignment of the Fe moment to its initial hard axis. Figure 2(c) shows the typical hysteresis loops under the maximum field strength of 200 Oe, which is well below the splitting field. Thus under the 200 Oe field, the Fe magnetization only deviated slightly from its easy axis due to the strong in-plane uniaxial anisotropy, as indicated in Fig. 1(e). It is clear that such a small field could also gradually switch the hysteresis loops from the HA loops into the EA

loops, as indicated by the 90° switching of CoO AFM domains. It should be noted that such AFM domain switching under the sweeping field of 200 Oe occurs at $T = 173$ K, much higher than that in Figs. 2(b) and 2(c), and this indicated that CoO domain switching encountered a higher energy barrier at the lower field, thus requiring larger thermal activation at higher temperature.

In order to understand the CoO AFM domain switching process, we studied the evolution of the ratio between the remanence Kerr signal (M_r) and the saturation signal (M_S) along the Fe hard axis [Figs. 2(d)–2(f)], which has been proven to be proportional to the fractional area of switched CoO AFM domains [23,30]. This switched CoO AFM domain area increases slowly with the cycling number at the beginning, faster in the middle, and then slowly again to approach the final saturation value of 1. The switching of the CoO AFM domain should involve a combination process of domain nucleation and growth, which can be described by the Kolmogorov-Avrami (KA) model [4,23,31,32]. Therefore, the CoO domain switching process can be described by exponential formula

$$M_r(N)/M_S = 1 - \exp(N/\tau_D)^\sigma. \qquad (1)$$

Here N is the number of field cycles and σ is the power index of the exponential function. τ_D is the relaxation time constant characterizing the typical time for CoO domain switching which has the unit of the time cost T_0 in each loop scan, and in our measurement, T_0 usually is $\sim$10 s. Excellent agreement between Eq. (1) and the experimental data in Figs. 2(d)–2(f) prove that the KA model is valid for describing the CoO AFM domain switching process.

In the Kolmogorov-Avrami model, the parameter τ_D represents the relaxation time constant, thus the temperature-dependent τ_D can provide the energy barrier of CoO AFM domain switching based on the Arrhenius law:

$$\tau_D = \tau_0 \exp(E_b/k_B T). \qquad (2)$$

Here, τ_0 is the characteristic attempt time with the unit of T_0 in our measurements, E_b is the energy barrier of the CoO AFM domain switching, and k_B is the Boltzmann constant. By fitting the data in Fig. 3(a), we can obtain the energy barrier for Fe (25 nm)/CoO (5 nm) under a sweeping field of 600 Oe to be $E_b = 0.99$ eV, which is comparable to that of other AFM materials such as NiO, IrMn, and NiMn discussed in Ref. [19].

To understand field-dependent CoO AFM domain switching and the energy barrier, we studied the relaxation time τ_D at different temperatures and various ranges of sweeping magnetic field, as shown in Fig. 3(b). CoO AFM domains show higher thermal stability at lower magnetic field, consistent with the fact of the smaller circling number at higher sweeping field measured at the same temperature. By fitting τ_D in Fig. 3(b) using Eq. (2), we can obtain the energy barrier E_b as a function of magnetic field, which saturates at low field range ($H < H_S \approx 350$ Oe) and decreases for stronger sweeping field. This result shows that AFM domain thermal stability in the Fe/CoO system also depends on the applied magnetic field.

The power index σ is $\sim$3 at high magnetic field, and increases at a lower field smaller than H_S. σ is associated with the exponent value of the power-law function describing domain growth as a function of time [4], and in Eq. (1),
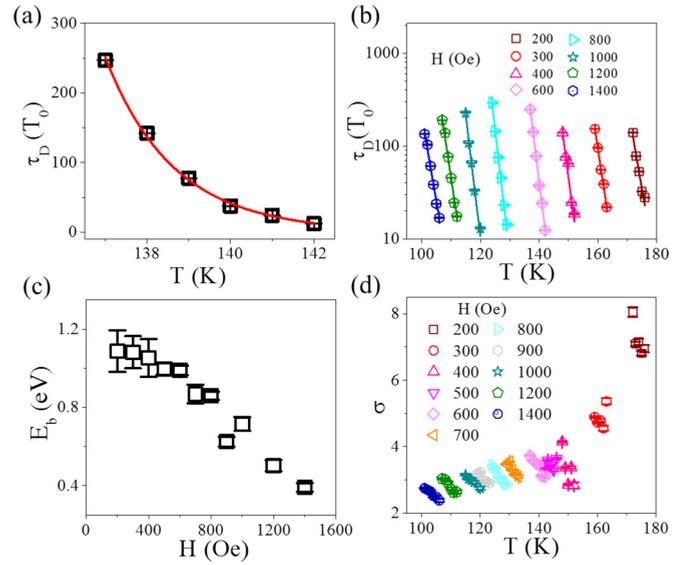

FIG. 3. (a) Temperature-dependent relaxation time constant τ_D using sweeping field range of 600 Oe of sample Fe (25 nm)/CoO (5 nm)/MgO(001). The red line is the fitted result using Eq. (2) based on the Arrhenius law. (b) Temperature-dependent relaxation time constant τ_D and (d) the fitted exponent σ at various magnetic fields. Lines in panel (b) are fitted results using Eq. (2). (c) The fitted energy barrier using Eq. (2) as a function of magnetic field. The unit T_0 of τ_D is the time cost ($\sim$10 s) of each loop scan in our measurements. The error bars are obtained during the fitting using Eqs. (1) and (2).

the value of σ determines how stretched or compressed the exponential relaxation curve is, thus the σ value indicates the relative contribution from domain wall motion over that from domain nucleation. For the reversal dynamics of FM domains, a value of $\sigma \sim 3$ corresponds to a domain wall motion dominated process [4]. Thus, we attribute our $\sigma \sim 3$ value at high magnetic field to the domain wall motion dominated CoO domain switching process, which coincides with the mechanism of AFM domain switching in Fe (23 nm)/CoO (5 nm) using a sweeping field of 700 Oe in Ref. [22]. A larger value of σ in a smaller field indicates even more dominance of domain wall motion over domain nucleation. This point is also reflected in the shape of the remanent Kerr signal change curve in Figs. 2(d)–2(f), where Fig. 2(f) under 200 Oe field sweeping has a steeper slope in the middle process than Fig. 2(d) under 900 Oe and Fig. 2(e) under 1000 Oe field sweeping. The change of the remanent Kerr signal at the beginning is usually attributed to the nucleation of new CoO AFM domains, while the domain change in the middle process is contributed by both the domain nucleation and domain wall motion [1,3,4], but may be dominated by the domain wall motion.

To better understand the effect of magnetic field on AFM domain switching, we performed magnetic domain imaging measurements using a Kerr microscope on a sample of Fe (25 nm)/CoO (4 nm)/MgO (001). First, the sample was cooled down with $H_{FC} \parallel y$, to align CoO spin with $S_{CoO} \parallel x$ and easy axis of the Fe layer with EA $\parallel y$. As shown in Figs. 4(a) and 4(e), a single domain with $M_{Fe} \parallel y$ appeared after field cooling. Remanent domain images were then taken after applying a positive field $+H$ and a negative field $-H$ at
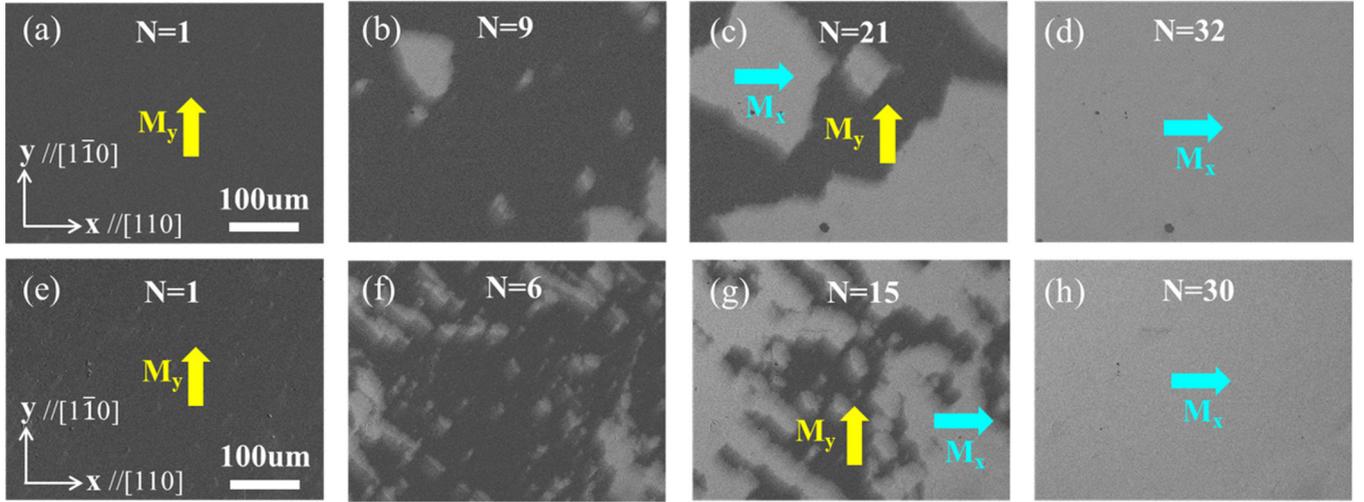
FIG. 4. Time-dependent domain evolution of Fe (25 nm)/CoO (4 nm)/MgO (001) at remanent state after different numbers of field cycling with [(a)–(d)] H decreased from 200 Oe at 163 K and [(e)–(h)] H decreased from 500 Oe at 144 K. The cycling number N is listed in each frame.

different numbers of cycles along the Fe hard axis ($H \parallel x$). Here, Figs. 4(a)–4(d) [top row] show the remanent domain images with magnetic field decreasing from +200 Oe to zero and Figs. 4(e)–4(h) [bottom row] show the remanent domain images with magnetic field decreasing from +500 Oe to zero. After several field cycles, new nucleated domains with $M_{Fe} \parallel x$ appeared randomly and finally expanded all over the film. Since Fe spin and CoO spin are strongly coupled together, the switch of the Fe easy axis from EA $\parallel y$ to EA $\parallel x$ at zero field corresponds to the switch of CoO spin from $S_{CoO} \parallel x$ to $S_{CoO} \parallel y$ [23,30]. Figures 4(a)–4(d) display CoO domain switching under 200 Oe, which is dominated by domain growth based on a few nucleated domains, whereas Figs. 4(e)–4(h) show more new nucleated small domains accompanying domain wall motion for CoO domain switching under 500 Oe. This experiment clearly demonstrates the difference of the CoO AFM domain switching mechanism under different ranges of field sweeping in the exchange-coupled Fe/CoO bilayer.

The contribution of domain nucleation and domain wall motion changes with magnetic field in the CoO AFM domain switching process, thus a clear clarification of these two mechanisms is strongly needed. In the earlier mentioned KA model used to describe the FM reversal process [4,23,31,32], the relaxation time τ_D and the power index σ depend on parameter k, which is $k = v/Rr_C$. Here v is the domain wall motion speed, R is the domain nucleation rate, and r_C is the radius of the nuclei [1,4]. However, the two mechanisms of domain nucleation and domain wall motion cannot be well separated from this extended exponential approximation fitting, as in Eq. (1). In order to understand the different role of the magnetic field, we tried to develop a new analysis method to distinguish the contribution of AFM domain nucleation and the contribution of domain wall motion through the remanent Kerr signal change. In this method, the nucleation process and domain wall motion are considered together, where a new domain is formed by the nucleation rate η_{DN} per unit area during each field cycling and the AFM spin at the domain boundary switching at the rate of η_{DW} per unit area during each

field cycling, which leads to the wall motion of the existing domain. Then the switched domain area ΔS within each field cycle is given by

$$\Delta S = \eta_{DN} \times (1 - S) + \eta_{DM} L(S). \tag{3}$$

Here S is the area with the switched CoO AFM spin and the total area under examination is normalized to 1. Since domain nucleation occurs randomly at the place of the nonswitched spin, the first term on the right side of the equation describes the domain nucleation process [3] and indicates that the nucleation possibility is proportional to the area of the unswitched CoO spins. The second term is ascribed to the wall motion process. Since domain wall motion could only occur at the domain boundary, the switching AFM domain area due to the domain wall motion is considered to be proportional to the length of the domain wall boundary L, which should be a function of S [3]. The relation between L and S could be complicated depending on the microscopic domain evolution process. The domain wall length L should be zero before and after the domain switching process, and can be expected to reach its maximum value if the half area is switched. So we propose that $L(S)$ is proportional to $[S(1 - S)]^n$, indicating that L is a power function of the macroscopic switched domain area considering that the boundary is formed between the switched and nonswitched domains. By substituting $L(S)$ with $[S(1 - S)]^n$, we obtain

$$\Delta S = \eta_{DN}(1 - S) + \eta_{DM}[S(1 - S)]^n. \tag{4}$$

We found the experimental data has a good fit with Eq. (4) by choosing the proper value of exponent n in the range of 0.7–1.3, as shown in Fig. 5(a). The variance of calculation from the experimental data is shown in the inset of Fig. 5(a), which shows the best n value is around 1. Interestingly, for $n = 1$, Eq. (4) happens to have the analytical solution

$$S = \frac{1 - e^{-N(\eta_{DN} + \eta_{DM})}}{1 + \frac{\eta_{DP}}{\eta_{DM}} e^{-N(\eta_{DN} + \eta_{DM})}}. \tag{5}$$
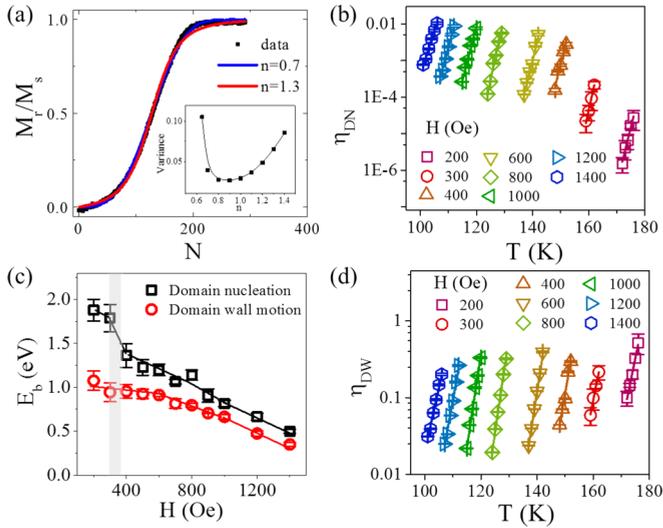
FIG. 5. (a) The change of remanent Kerr signal with field cycling number from Fe (25 nm)/CoO (5 nm)/MgO(001) using 800 Oe of field range at 124 K. Red and blue curves are numerical calculations with $n = 0.7$ and $n = 1.3$, respectively. The inset gives the variance of the calculated data using Eq. (4) from the experimental data as a function of power index n. Temperature-dependent (b) domain nucleation rate and (d) domain wall motion rate at various magnetic fields. (c) Energy barrier for both domain nucleation and domain wall motion as a function of magnetic field.

So in the following analysis, we only consider the situation with $n = 1$. The nucleation rate η_{DN} and domain wall motion rate η_{DW} for the CoO AFM domain switching process are obtained through fitting of experimental data. Figures 5(b) and 5(d) show explicitly the temperature-dependent η_{DN} and η_{DW} at different maximum magnetic fields during the field sweeping process. We found η_{DN} to be about two orders smaller than η_{DW} for $H > H_S \approx 350$ Oe, and four orders smaller for $H < H_S$. All of the temperature-dependent η_{DN} and η_{DW} can be well described by the Arrhenius law

$$\eta = \eta_0 \exp(-E_b/k_B T). \qquad (6)$$

Here η_0 is the characteristic spin switching rate. The fittings in Figs. 5(b) and 5(d) yield the energy barriers E_b^{DN} and E_b^{DM} for domain nucleation and domain wall motion as a function of magnetic field, as shown in Fig. 5(c). For $H > H_S \approx 350$ Oe, both E_b^{DN} and E_b^{DM} decrease with H, and E_b^{DM} is always less than E_b^{DN}, indicating that domain wall motion dominates the AFM domain switching process. However, while decreasing the field H to about 350 Oe, E_b^{DN} shows a clear jump, while E_b^{DM} only slightly increases at lower field. The difference between E_b^{DN} and E_b^{DM} becomes larger for $H \leqslant 350$ Oe, so the domain wall motion becomes more dominant in the AFM domain switching process, consistent with the domain evolution process measured with the Kerr microscope shown in Fig. 4. It should be noted that the energy barrier determined by the Kolmogorov-Avrami model shown in Fig. 3(d) is only slightly larger than the energy barrier E_b^{DM} of domain wall motion, and this is very reasonable since the KA model describes the effective energy barrier of the domain switching process dominated by domain wall motion in our system.
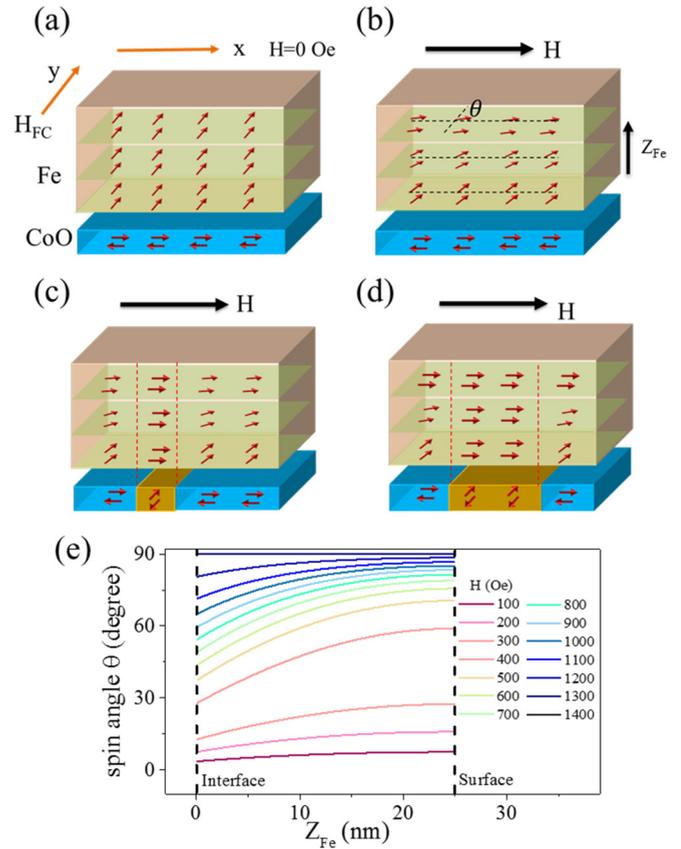

FIG. 6. Schematic drawing of the spin configuration (a) after field cooling, (b) applying magnetic field along x, (c) domain nucleation, and (d) domain wall motion of the CoO layer in the Fe/CoO system. The switched CoO spins are highlighted in yellow. The boundary of switched CoO spins and Fe spins on the top are shown with a dashed line. (e) Spin profile of the Fe layer under various magnetic fields along the x direction by micromagnetic simulation. The spin angle θ is defined as the angle between the y axis and the spins in each Fe layer, as shown in (b). All the Fe and CoO spins in different layers are in the $x - y$ plane.

Next, we should understand why the CoO AFM spin switching energy barrier can be influenced by the magnetic field, since usually the spins in the AFM layer should not respond to the magnetic field. It should be noted that the 90° switching of the CoO AFM domain occurs with the field along the hard axis, and it is the exchange coupling at the Fe/CoO interface driving the switch of the CoO AFM spins. The measured field-dependent energy barrier indicates that the effective exchange coupling changes with the field strength. The interface coupling in the Fe/CoO(001) system should make the Fe and CoO spins perpendicularly coupled due to the spin-flop coupling, thus after field cooling along the Fe⟨100⟩ direction, the CoO AFM spins were set perpendicular to the cooling field H_{FC}, as shown in Fig. 6(a). The exchange-coupling-induced anisotropy should locate at the interface, thus the Fe spins at the interface contain a very strong uniaxial anisotropy, different with the other Fe spins away from the interface. When the field was applied perpendicular to H_{FC}, the surface Fe spins could follow along the field direction and the strong interface anisotropy could drive the interface Fe

spins away from the field direction, forming a vertical spin spiral in the Fe film, as indicated in Fig. 6(b). The orientation angle θ, defined as the angle between the Fe spin and H_{FC}, varies with the layer position of the Fe spins and also changes with the applied field strength. However, if the CoO spins switch by 90°, the easy axis of the exchange-coupling-induced anisotropy should switch to the field direction. Thus if a 90° AFM domain nucleates as shown in Fig. 6(c), the Fe spins on top of this switched CoO domain should fully align along the field direction. The energy of the spin configuration in Fig. 6(c) could be less than that in Fig. 6(b) due to the lower Zeeman energy, then the thermal activation could generate the new CoO AFM domains with a lower system energy. After domain nucleation, the AFM anisotropy energy in the final state is the same as that in the initial state due to the fourfold AFM anisotropy, but the AFM domain wall will cost the additional exchange energy. In the Fe layer, after CoO AFM domain formation, the Fe film will increase the lateral domain wall energy, but reduce the vertical exchange energy by reducing the area of the vertical spin spiral. It should be noted that the force driving the CoO AFM spins across the AFM anisotropy barriers is the interface exchange coupling, the strength of which is related to the angle between the CoO AFM spins and the Fe FM spins at the interface. The spin angles in the Fe film can be strongly influenced by the external field, thus the interface Fe spins could be more parallel to the x axis at the stronger field, which could align the CoO spins to the y axis, so that the resulting thermally activated energy barrier for CoO domain nucleation is lower for the stronger field. Moreover, the system energy can be further reduced by expanding the AFM domain through the domain wall motion. Figure 6(d) shows the schematic spin configuration for an expanding AFM domain due to the domain wall motion from an existing AFM domain. Compared with domain nucleation, AFM spin may overcome less exchange-coupling energy between CoO-CoO during the domain wall motion process. Thus, it is understandable that the measured energy barrier of domain wall motion in Fig. 5(c) is always less than that of the domain nucleation.

The vertical spin spiral in Fig. 6(b) can be confirmed by the micromagnetic simulation based on the standard OOMMF package [33]. In the simulation, we assumed that the exchange coupling at the Fe/CoO interface created a constant strong interface uniaxial anisotropy on the interfacial Fe layer, thus the interface Fe layer contains both exchange-coupling-induced uniaxial anisotropy and cubic anisotropy, and the other Fe layer only contains a cubic anisotropy [23,25,34]. If assuming the cooling field is along the y axis, the easy axis of the interfacial uniaxial anisotropy is along the x axis with the strength of $J_{Fe-CoO} = H_S M_S d_{Fe} \approx 1.5$ erg/cm^2 [25]. The cubic anisotropy of $K_{4,Fe} = 4.5 \times 10^5$ erg/cm^3 with easy axis along the x and y axes [34], exchange stiffness of 15×10^{-12} J/m, saturation magnetization of 1714 emu/cm^3, and thickness of 25 nm were used for Fe layers in the simulation. The lateral dimension of 60×60 nm^2 with the two-dimensional periodic boundary condition was applied in the simulation. The unit cell size was chosen as $1 \times 1 \times 0.2$ nm^3. Note that the uniaxial interfacial anisotropy should locate in the Fe atomic layer at the Fe/CoO interface, so to better simulate the interface character of this interfacial uniaxial anisotropy, the unit cell along z axis was chosen as 0.2 nm, which is close to the layer thickness

$a_{Fe} = 0.143$ nm of the Fe film. Figure 6(e) shows the spin orientation angle θ at different layer positions with different field strengths, and here θ is defined as the angle between the y axis and the spins in each Fe layer. It is clear that θ changes with the layer position, confirming the existence of the vertical spin spiral in the Fe layer. Moreover, the calculated results show that the spin orientation changes quickly around 350 Oe, indicating that the observed energy barrier change around H_S in Fig. 5(c) is related to the magnetic spin structure in Fe film. It should be pointed out that the driving force to create a new AFM domain is the interface coupling at the Fe/CoO interface, thus the strong change of the measured energy barrier of domain wall nucleation in Fig. 5(c) should be attributed to the change of the interfacial Fe spin orientation at H_S. However, the measured energy barrier due to the domain wall motion does not show obvious change around H_S in Fig. 3(c). The AFM domain wall motion happens below the FM domain wall, and our simulation cannot obtain the field-dependent spin structure inside the FM domain wall, which should be much different with that inside a FM domain. For a magnetic field smaller than H_S but larger than H_C, a ferromagnet on top of switched CoO spin is always aligned parallel to the magnetic field direction while a ferromagnet on top of unswitched CoO spin tilts toward the magnetic field direction at an angle, thus forming a lateral domain wall within Fe layer. In this way, the interfacial Fe spin orientation within the Fe domain wall does not exhibit abrupt change for the magnetic field across H_S. It should be noted that in micromagnetic simulations, we could not consider the change of the CoO AFM spin configuration with the applied field, and the AFM spin configuration would also be important for understanding the nucleation and wall motion of the AFM domains.

IV. SUMMARY

In summary, we investigated field-dependent AFM spin switching in epitaxially grown Fe/CoO/MgO(001). MOKE hysteresis loops and Kerr microscopy demonstrated that the energy barrier decreased at larger magnetic field. AFM domain switching occurred even for $H < H_S$, where the Fe moment is not fully driven along the field direction, and the domain wall motion of the nucleated AFM domain is dominant in the CoO AFM spin switching process. To explain different behaviors of the magnetic-field-dependent energy barrier for domain nucleation and domain wall motion across H_S, a new analytical method was proposed to separate these two mechanisms. Micromagnetic simulation confirmed the formation of a spiral-like spin configuration in the Fe layer, and the field-dependent behavior of the energy barrier was attributed to the interface exchange coupling between FM and AFM spins. This work sheds light on a way to control the AFM spin switching process layer using magnetic fields.

[1] J. Pommier, P. Meyer, G. Penissard, J. Ferre, P. Bruno, and D. Renard, Phys. Rev. Lett. **65**, 2054 (1990).

[2] W. Wernsdorfer, E. Bonet Orozco, K. Hasselbach, A. Benoit, B. Barbara, N. Demoncy, A. Loiseau, H. Pascard, and D. Mailly, Phys. Rev. Lett. **78**, 1791 (1997).

[3] S.-B. Choe and S.-C. Shin, Phys. Rev. Lett. **86**, 532 (2001).

[4] H. W. Xi, K.-Z. Gao, J. O. Yang, Y. M. Shi, and Y. Z. Yang, J. Phys.: Condens. Matter **20**, 295220 (2008).

[5] A. Kirilyuk, J. Ferŕe, V. Grolier, J. P. Jamet, and D. Renard, J. Magn. Magn. Mater. **171**, 45 (1996).

[6] J. Ferŕe, J. P. Jamet, and P. Meyer, Phys. Status Solidi A **175**, 213 (1999).

[7] M. Yamanouchi, J. Ieda, F. Matsukura, S. E. Barnes, S. Maekawa, and H. Ohno, Science **317**, 1726 (2007).

[8] K.-J. Kim, J. Ryu, G.-H. Gim, J.-C. Lee, K.-H. Shin, H.-W. Lee, and S.-B. Choe, Phys. Rev. Lett. **107**, 217205 (2011).

[9] K.-J. Kim, J.-C. Lee, S.-M. Ahn, K.-S. Lee, C.-W. Lee, Y. J. Cho, S. Seo, K.-H. Shin, S.-B. Choe, and H.-W. Lee, Nature (London) **458**, 740 (2009).

[10] A. Stupakiewicz, E. Y. Vedmedenko, A. Fleurence, T. Maroutian, P. Beauvillain, A. Maziewski, and R. Wiesendanger, Phys. Rev. Lett. **103**, 137202 (2009).

[11] J. Nogués and I. K. Schuller, J. Magn. Magn. Mater. **192**, 203 (1999).

[12] B. G. Park, J. Wunderlich, X. Martí, V. Holý, Y. Kurosaki, M. Yamada, H. Yamamoto, A. Nishide, J. Hayakawa, H. Takahashi, A. B. Shick, and T. Jungwirth, Nat. Mater. **10**, 347 (2011).

[13] X. Marti, I. Fina, C. Frontera, J. Liu, P. Wadley, Q. He, R. J. Paull, J. D. Clarkson, J. Kudrnovský, I. Turek, J. Kuneš, D. Yi, J.-H. Chu, C. T. Nelson, L. You, E. Arenholz, S. Salahuddin, J. Fontcuberta, T. Jungwirth, and R. Ramesh, Nat. Mater. **13**, 367 (2014).

[14] Stephen M. Wu, W. Zhang, A. KC, P. Borisov, J. E. Pearson, J. S. Jiang, D. Lederman, A. Hoffmann, and A. Bhattacharya, Phys. Rev. Lett. **116**, 097204 (2016).

[15] H. Wang, C. Du, P. C. Hammel, and F. Yang, Phys. Rev. Lett. **113**, 097202 (2014).

[16] W. W. Lin, K. Chen, S. F. Zhang, and C. L. Chien, Phys. Rev. Lett. **116**, 186601 (2016).

[17] L. Frangou, S. Oyarzún, S. Auffret, L. Vila, S. Gambarelli, and V. Baltz, Phys. Rev. Lett. **116**, 077203 (2016).

[18] D. Qu, S. Y. Huang, and C. L. Chien, Phys. Rev. B **92**, 020418(R) (2015).

[19] H. W. Xi, Scott Franzen, S. N. Mao, Robert, and M. White, Phys. Rev. B **75**, 014434 (2007).

[20] J. Dho, C. W. Leung, and M. G. Blamire, J. Appl. Phys. **99**, 033910 (2006).

[21] P. A. A. van der Heijden, T. F. M. M. Maas, W. J. M. de Jonge, J. C. S. Kools, and F. Roozeboom, Appl. Phys. Lett. **72**, 492 (1998).

[22] S. Polisetty, S. Sahoo, and C. Binek, Phys. Rev. B **76**, 184423 (2007).

[23] Q. Li, G. Chen, T. P. Ma, J. Zhu, A. T. N'Diaye, L. Sun, T. Gu, Y. Huo, J. H. Liang, R. W. Li, C. Won, H. F. Ding, Z. Q. Qiu, and Y. Z. Wu, Phys. Rev. B **91**, 134428 (2015).

[24] P. Wadley, B. Howells, J. Železný, C. Andrews, V. Hills, R. P. Campion, V. Novák, K. Olejník, F. Maccherozzi, S. S. Dhesi, S. Y. Martin, T. Wagner, J. Wunderlich, F. Freimuth, Y. Mokrousov, J. Kuneš, J. S. Chauhan, M. J. Grzybowski, A. W. Rushforth, K. W. Edmonds, B. L. Gallagher, and T. Jungwirth, Science **351**, 587 (2016).

[25] J. Zhu, Q. Li, J. X. Li, Z. Ding, C. Y. Won, and Y. Z. Wu, J. Appl. Phys. **114**, 173912 (2013).

[26] W. N. Cao, J. Li, G. Chen, J. Zhu, C. R. Hu, and Y. Z. Wu, Appl. Phys. Lett. **98**, 262506 (2011).

[27] J. Wu, J. S. Park, W. Kim, E. Arenholz, M. Liberati, A. Scholl, Y. Z. Wu, C. Hwang, and Z. Q. Qiu, Phys. Rev. Lett. **104**, 217204 (2010).

[28] N. C. Koon, Phys. Rev. Lett. **78**, 4865 (1997).

[29] T. C. Schulthess and W. H. Butler, Phys. Rev. Lett. **81**, 4516 (1998).

[30] F. Nolting, A. Scholl, J. Stöhr, J. W. Seo, J. Fompeyrine, H. Siegwart, J.-P. Locquet, S. Anders, J. Lüning, E. E. Fullerton, M. F. Toney, M. R. Scheinfeink, and H. A. Padmore, Nature (London) **405**, 767 (2000).

[31] A. N. Kolmogorov, Izv. Akad. Nauk SSSR, Ser. Matem. **3**, 355 (1937).

[32] M. Avrami, J. Chem. Phys. **8**, 212 (1940).

[33] M. J. Donahue and D. Porter, OOMMF (NIST), http://math.nist.gov/oommf.

[34] G. Chen, J. Zhu, J. Li, F. Z. Liu, and Y. Z. Wu, Appl. Phys. Lett. **98**, 132505 (2011).